American Journal of Pathology, Vol. 168, No. 2, February 2006

DOI: 10.2353/ajpath.2006.050404

Lithocholic Acid Feeding Induces Segmental Bile Duct Obstruction and Destructive Cholangitis in Mice

Peter Fickert,* Andrea Fuchsbichler,† Hanns-Ulrich Marschall,‡ Martin Wagner,* Gernot Zollner,* Robert Krause,* Kurt Zatloukal,† Hartmut Jaeschke,§ Helmut Denk,† and Michael Trauner*

From the Laboratory of Experimental and Molecular Hepatology, Division of Gastroenterology and Hepatology, Department of Medicine, and Department of Pathology,† Medical University, Graz, Austria; the Karolinska University Hospital Huddinge,‡ Stockholm, Sweden; and the Liver Research Institute,§ University of Arizona, Tucson, Arizona*

We determined the mechanisms of hepatobiliary injury in the lithocholic acid (LCA)-fed mouse, an increasingly used model of cholestatic liver injury. Swiss albino mice received control diet or 1% (w/w) LCA diet (for 1, 2, and 4 days), followed by assessment of liver morphology and ultrastructure, tight junctions, markers of fibrosis and key proteins of hepatobiliary function, and bile flow and composition. As expected LCA feeding led to bile infarcts, which were followed by a destructive cholangitis with activation and proliferation of periductal myofibroblasts. At the ultrastructural level, small bile ducts were frequently obstructed by crystals. Biliary-excreted fluorescence-labeled ursodeoxycholic acid accumulated in bile infarcts, whereas most infarcts did not stain with India ink injected into the common bile duct; both findings are indicative of partial biliary obstruction. Expression of the main basolateral bile acid uptake proteins (sodium-taurocholate cotransporter and organic anion-transporting polypeptide 1) was reduced, the canalicular transporters bile salt export pump and multidrug-related protein 2 were preserved, and the basolateral transporter multidrug-related protein 3 and the detoxifying enzyme sulfotransferase 2a1 were induced. Thus, we demonstrate that LCA feeding in mice leads to segmental bile duct obstruction, destructive cholangitis, periductal fibrosis, and an adaptive transporter and metabolic enzyme response. ***(Am J Pathol 2006, 168:410–422; DOI: 10.2353/ajpath.2006.050404)***

The effects of the monohydroxy bile acid lithocholic acid (LCA) have been studied in rodents (ie, mainly in the rat, hamster, and rabbit) since the early 1960s to understand the role of potentially hepatotoxic bile acids in the pathogenesis of cholestatic liver injury.[1–4] The proposed concepts on the pathogenesis of LCA-induced cholestasis in rodents (ie, mainly rats) include biochemical alterations of the bile canalicular membrane,[5,6] the development of crystalline plugs in bile canaliculi due to the poor solubility of LCA,[3,7] and impaired trafficking or increased retrieval of canalicular export pumps to and from the canalicular membrane.[8,9] In addition, LCA is increasingly being investigated in (knockout) mice to clarify the role of hepatic metabolic phase I and II detoxifying enzymes and their regulatory nuclear receptors in the hepatic defense against toxic bile acids.[10–15] However, the cholestatic phenotype and the pathogenesis of hepatobiliary injury of LCA-treated mice are still poorly understood.

Potentially toxic bile acids may affect not only hepatocytes but also bile duct epithelial cells (cholangiocytes).[16] Under physiological conditions, bile acids and biliary phospholipids are transported into bile via the bile salt export pump (Bsep/Abcb11) and the canalicular phospholipid flippase (multidrug resistance gene 2 [Mdr2]/Abcb4), respectively, and subsequently form mixed micelles, which protect cholangiocytes from bile acid toxicity.[17] We have previously described the development of sclerosing cholangitis in mice with targeted disruption of the *Mdr2* gene and subsequent absence of biliary phospholipid secretion.[18,19] This results in an in-

Supported by grants P-15502 (to M.T.) from the Austrian Science Foundation and a GEN-AU project grant from the Austrian Ministry for Science (to M.T.).

Accepted for publication October 6, 2005.

Address reprint requests to Michael Trauner, M.D., Laboratory of Experimental and Molecular Hepatology, Division of Gastroenterology and Hepatology, Department of Internal Medicine, Medical University Graz, Auenbruggerplatz 15, A-8036 Graz, Austria. E-mail: michael.trauner@meduni-graz.at.

creased biliary concentration of monomeric bile acids, causing bile duct injury, pericholangitis followed by onion skin type periductal fibrosis, and finally chronic sclerosing cholangitis.[19,20] In addition, these mice are also prone to form cholesterol crystals and stones.[20] We therefore tested the hypothesis that an increased biliary concentration of a potentially toxic and lithogenic bile acid (ie, LCA) leads to bile duct injury and cholangitis even in the presence of normal phospholipid secretion.

Materials and Methods

Animal Experiments

Experiments were performed with 2-month-old male mice weighing 25 to 30 g. To assess potential strain differences in the susceptibility to toxic liver injury, the time course of LCA-induced liver injury was studied in four different mouse strains (Swiss albino, FVB/N, C57/Bl6, and 129 SV) by feeding a 1% LCA-supplemented diet for 1 to 4 days. This dose was chosen because feeding 0.5% supplemented diet in a pilot study did not result in a cholestatic phenotype as described below. All tested mouse strains developed a comparable cholestatic phenotype (as outlined in Results) and all subsequent studies were performed in Swiss albino mice. Mice were housed with a 12:12 hour light:dark cycle and permitted *ad libitum* consumption of water. Controls were fed a standard mouse diet (Sniff, Soest, Germany). The experimental protocols were approved by the local Animal Care and Use Committee according to criteria outlined in the Guide for the Care and Use of Laboratory Animals prepared by the National Academy of Sciences, as published by the National Institutes of Health (NIH publication 86-23, revised 1985). Serum biochemical analysis, liver histology, electron microscopy, and immunohistochemisty for α-smooth muscle actin (α-SMA) were performed as described previously.[19,21]

Immunohistochemistry for CD11b

To characterize the inflammatory infiltrate, CD11b-positive cells (neutrophils) were detected as described previously[19] with the modification that binding of the antibody was detected using the ABC system (Dako, Glostrup, Denmark) using β-amino-9-ethyl-carbazole (AEC; Dako) as substrate.

Immunohistochemistry for Proliferation Marker Ki-67

Immunohistochemistry for Ki-67 was performed on microwave-treated paraffin sections (4 μm thick) using 0.01 mmol/L citrate buffer (pH 6.0) and a polyclonal rabbit anti-Ki-67 antibody (dilution 1:500; Novocastra, Newcastle on Tyne, UK). Binding of the antibody was detected using the ABC system (Dako) with AEC (Dako) as substrate.

Immunohistochemistry for Cytokeratin 19 (CK19)

Immunohistochemistry for CK19 was performed on cryosections fixed with a modified formalin/methanol/acetone fixation. In brief, sections were fixed in 4% buffered formaline for 5 minutes and then fixed with methanol for 5 minutes at −20°C and with acetone for 3 minutes at −20°C. CK19 was detected using the monoclonal rat anti-Troma-III antibody (developed by Rolf Kemler, Max Planck Institute, Freiburg, Germany), which was obtained from the Developmental Studies Hybridoma Bank (developed under the auspices of the National Institute of Child Health and Human Development and maintained by the University of Iowa, Iowa City, IA). Binding of the antibody was detected using the ABC system (Dako) with AEC (Dako) as substrate.

Bile Flow and Composition

Bile flow was determined as described previously.[21] Biliary phospholipid concentrations were determined using a commercially available kit (Phospholipid B; Wako, Neuss, Germany) according to the manufacturer's instructions. In detail, 5 μl of bile was mixed with 750 μl of color reagent and incubated for 10 minutes at 37°C and measured at 505 nm. Concentrations were determined using the standard solution of the kit. Biliary cholesterol concentrations were determined using a commercially available kit (cholesterol liquicolor; Human, Wiesbaden, Germany) according to the manufacturer's instructions. For cholesterol extraction, 5 μl of bile and 95 μl of distilled water were mixed with 400 μl of chloroform:methanol (2:1) and centrifuged 5 minutes at 14,000 $\times$ *g* The lower phase was concentrated, and the obtained pellet was dissolved in 5 μl of methanol. After the addition of 500 μl of color reagent and incubation at 37°C for 5 minutes, probes were measured at 500 nm. Concentration was determined using the standard solution of the kit. For biliary glutathione, proteins in bile were precipitated with 5% metaphosphoric acid (2.5 μl of bile in 50 μl of metaphosphoric acid), and glutathione analysis was performed using the glutathione assay kit (Calbiochem, San Diego, CA), according to the manufacturer's instructions. Biliary bile acid concentration required bile to be diluted 1:300 in physiological saline and analyzed using a 3α-hydroxysteroid dehydrogenase assay (Ecoline S^+; DiaSys, Holzheim, Germany) according to the manufacturer's instructions. Equipment and conditions used for extraction, electrospray mass spectrometry, and gas chromatography-mass spectrometry were the same as previously described.[18]

mRNA Analysis and Polymerase Chain Reaction of Transporters, Metabolic Enzymes, and Fibrosis Key Genes

RNA isolation, cDNA synthesis, and Taqman real-time polymerase chain reaction were performed as described

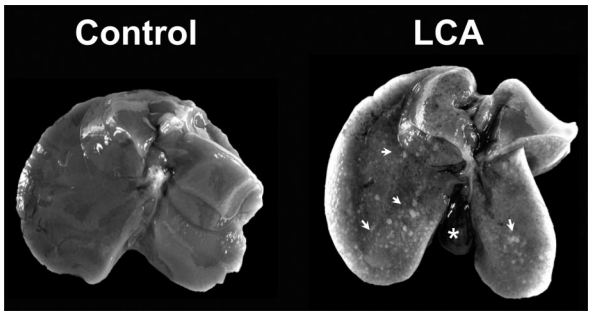

Figure 1. Macroscopic appearance of the liver in lithocholic acid-fed mice. Compared with the control liver on the **left**, the liver from a mouse fed a 1% (w/w) LCA-supplemented diet for 4 days is enlarged and shows numerous small necrotic areas (ie, bile infarcts) on its surface (indicated by **arrows**). Note also the enlarged gall bladder in the LCA-fed mouse liver (indicated by the **asterisk**).

previously.[22] The following primers and 5′-FAM, 3′-TAMRA-labeled probes were used: multidrug resistance-associated protein (Mrp2); bile salt export pump (Bsep); 28S rRNA[22]; Mrp3[23]; cytochrome p450 (Cyp) 3a11 fwd, 5′-CCACCAGTAGCACACTTTCC-3′; Cyp3a11 rev, 5′-TTC-CATCTCCATCACAGTATCA-3′; Cyp3a11 probe, 5′-CTCT-GCCCAACAAGGCACCTCC-3′; sulfotransferase (Sult) 2a1 fwd, 5′-GGAAGGACCACGACTCATAAC-3′; Sult2a1 rev, 5′-GATTCTTCACAAGGTTTGTGTTACC-3′; Sult2a1 probe, 5′-CCCATCCATCTCTTCTCCAAGTCTTTCTTCAG-3′; sodium-taurocholate cotransporter (Ntcp) fwd, 5′-CACCATG-GAGTTCAGCAAGA-3′; Ntcp rev, 5′-AGCACTGAGGGGC-ATGATAC-3′; Ntcp probe, 5′-AGGC-TCACTTCTGGAAGC-CCAAA-3′; collagen 1a1 (Col1a1) fwd, 5′-CAATGCAAT-GAAGAACTGGACTGT-3′; Col1a1 rev, 5′-TCCTACATCT-TCTGAGTTTGGTGA-3′; Col1a1 probe, 5′-CAGAAAGCA-CAGCACTCGCCCTCC-3′; tissue inhibitor of metallo-proteinases 1 (TIMP-1) fwd, 5′-CATGGAAAGCCTCTGTG-GATATG-3′; TIMP-1 rev, 5′-AA-GCTGCAGGCATTGATGT-G-3′; TIMP-1 probe, 5′-CTCA-TCACGGGCCGCCTAAG-GAAC-3′; matrix metallopro-teinase-2 (MMP-2) fwd, 5′-CTTTGAGAAGGATGGCAAGTATGG-3′; MMP-2 rev, 5′-

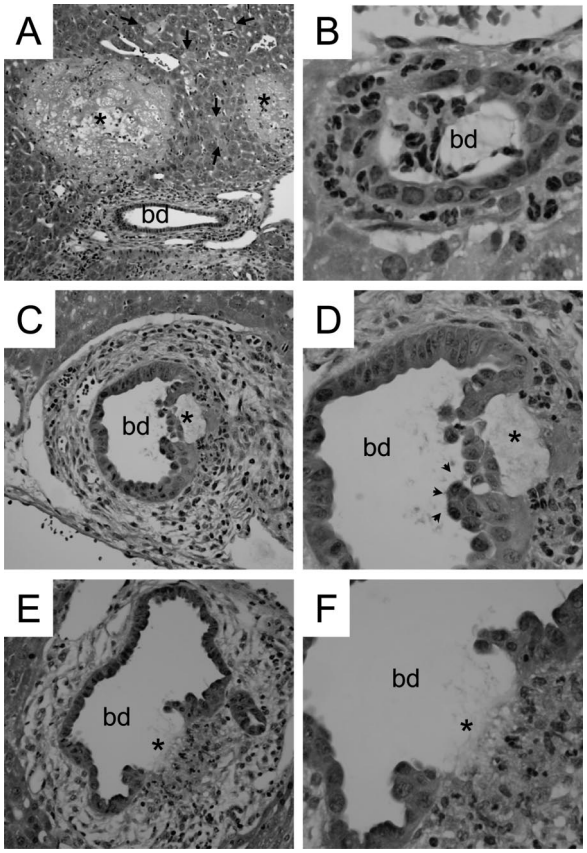

Figure 2. Lithocholic acid (LCA) feeding leads to bile infarcts and destructive cholangitis in mouse liver. Livers of mice fed 1% (w/w) LCA-supplemented diet for 2 days (**A**) and 4 days (**B–F**). **A:** Liver histology of a 2-day LCA-fed mouse reveals characteristic bile infarcts (**asterisks**) and disseminated single-cell necroses (**arrows**) in hepatic acinar zone 1 and 2. **B:** Small bile duct in 4-day LCA-fed mouse liver with pronounced cholangitis with numerous neutrophils surrounding and invading the bile duct. **C** and **D:** Larger bile duct with pronounced periductal edema, percholangitis, periductal fibrosis, and subepithelial fluid accumulation leading to detachment of biliary epithelium (**asterisk**). **Arrowheads** mark pseudopapillary proliferation of BECs. **E** and **F:** Bile duct with pericholangitis, periductal fibrosis, and ulceration of the bile duct epithelium (**asterisk**). Note also neutrophils invading the ulcer (**F**). bd, bile duct. hematoxylin and eosin staining; original magnification for **A,** ×10; for **B,** ×63; for **C** and **E,** ×20; for **D** and **F,** ×40.

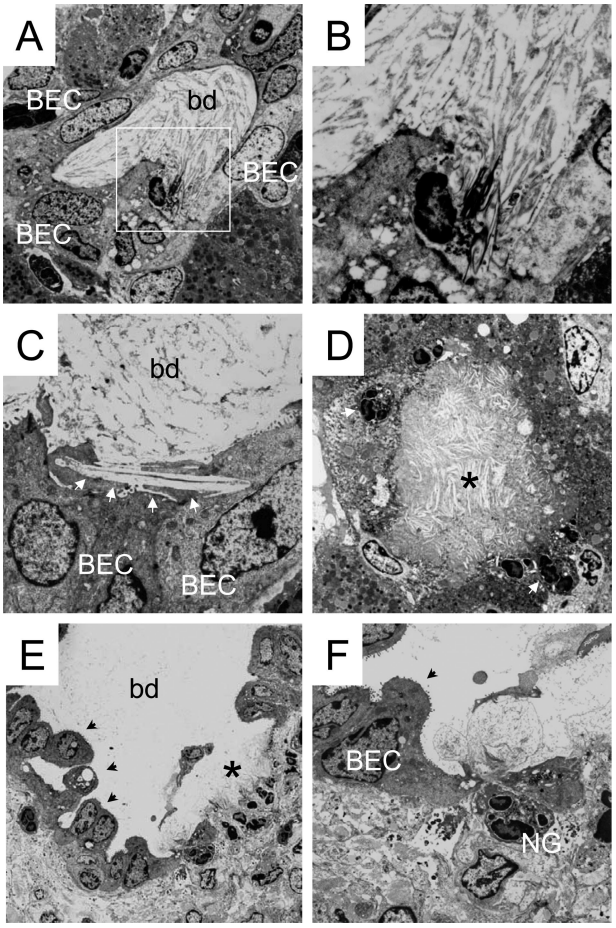

Figure 3. LCA feeding leads to obstruction of intralobular bile ducts by crystals, bile infarcts, and destructive cholangitis in mouse liver—ultrastructural characteristics. **A–F:** Electron microscopy from the liver of a 4-day LCA-fed mouse. **A:** Totally obstructed interlobular bile duct containing crystalline material. **B:** Larger magnification of the highlighted area of **A** shows crystals spearing BECs. **C:** Large crystal (indicated by the **arrowheads**) spearing BECs of an interlobular bile duct. **D:** Bile infarct (**asterisk**) containing crystalline material surrounded by severely altered hepatocytes and invading neutrophils (**arrowhead**). **E:** Interlobular bile duct with altered bile duct epithelium and ulceration (indicated by the **asterisk**). **Arrowheads** mark pseudopapillary proliferation of BECs. **F:** Higher magnification of the ulcer showing invading neutrophilic granulocytes (NG). bd, bile duct.

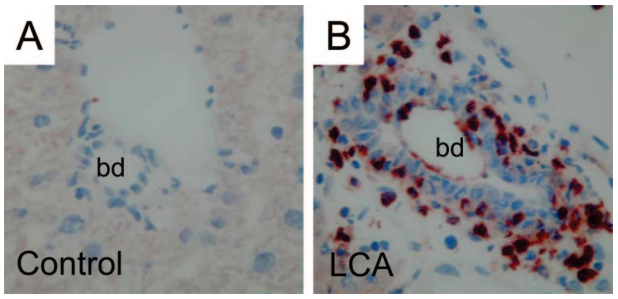

Figure 4. Characterization of the inflammatory infiltrate in LCA-fed mouse liver. Immunohistochemisty for CD11b (marker for neutrophils)-positive cells (red) in control liver (**A**) and liver from a 4-day LCA-fed mouse (**B**). **A:** Lack of CD11b staining in control liver. **B:** Inflammatory infiltrate in the portal tract of a 4-day LCA-fed mouse primarily consists of neutrophils (red). bd, bile duct. Original magnification for **A** and **B,** ×40.

TTGTAGGAGGTGCCCTGG-AA-3′; and MMP-2 probe, 5′-CAGATGGACAGCCCTGCAAGTTCCC-3′.

Preparation of Liver Membranes and Analysis of Transporter Protein Levels by Western Blotting

Liver membranes were prepared as described previously.[21] Transporter protein levels were determined using polyclonal antibodies against Bsep (dilution, 1: 7500; kindly provided by Dr. Renxue Wang, Vancouver, Canada), Mrp2 (dilution, 1: 1000; kindly provided by Dr. Bruno Stieger, Zurich, Switzerland), Mrp3 (dilution, 1: 1000; kindly provided by Dr. Dietrich Keppler, Heidelberg, Germany), Ntcp (dilution, 1: 2500; kindly provided by Dr. Bruno Stieger), and organic anion transporting protein (Oatp1) (dilution, 1: 1000; kindly provided by Dr. Bruno Stieger). Blots were reprobed with an anti-β-actin antibody (dilution, 1:5000; Sigma, Steinheim, Germany) to confirm the specificity of changes in transporter protein levels.[21,22,24]

Preparation of Total Liver Protein and Analysis of α-SMA Expression by Western Blotting

Protein was isolated by sonicating liver tissue in a homogenization buffer (0.25 mol/L sucrose, 10 mmol/L HEPES, pH 7.5, and 1 mmol/L EDTA, pH 8.0, containing protease inhibitors phenylmethylsulfonyl fluoride, aprotinin, leupeptin, and pepstatin). Protein (30 mg) was run on a 10% sodium dodecyl sulfate-polyacrylamide gel, transferred to nitrocellulose, and blotted with a monoclonal mouse antibody against a-SMA (dilution, 1:2000; Dako). Binding was detected using peroxidase-conjugated rabbit anti-mouse immunoglobulins (Dako). Determination of protein concentration, protein loading, and protein expression levels was performed as described previously.[21,22] Blots were reprobed with an anti-β-actin antibody (dilution, 1:5000; Sigma) to confirm the specificity of changes in α-SMA expression.

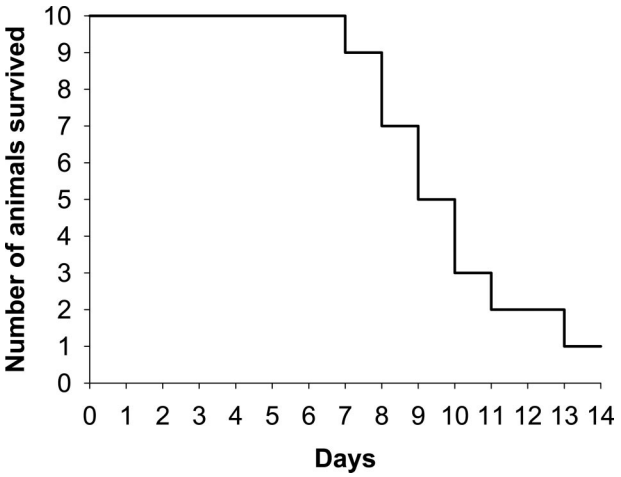

Figure 5. Prolonged feeding of 1% LCA-supplemented diet is not tolerable for mice. Kaplan-Meier curve. After 14 days of feeding 1% LCA-supplemented diet, only 1 of 10 animals is still alive.

Immunofluorescence Microscopy

Hepatocellular localization of the key basolateral (Ntcp and Mrp3) and canalicular (Mrp2 and Bsep) transporters, staining for cytokeratin 8/18 (CK8/18), CK19, laminin, and activated caspase-3 was studied by immunofluorescence microscopy as described previously.[18,21]

Lobular Distribution of India Ink and Fluorescent-Labeled Ursodeoxycholic Acid (UDCA)

India ink was injected into the common bile duct and visualized as previously described[18] to determine its lobular distribution in LCA-fed mice and for comparison in 3-day common bile duct ligated (CBDL)-mice.[18] To study a potential relationship between the cholestatic phenotype observed in LCA-fed mice and the lobular distribution of bile acids, fluorescent UDCA (UDC-lysyl-nitrobenzoxadiazolyl; kindly provided by Dr. Alan Hofmann, University of California, San Diego, La Jolla, CA) was injected into the inferior vena cava, and excreted fluorescent UDCA was viewed by fluorescence microscopy and compared with CBDL mice as described previously.[19]

Table 1. Serum Biochemistry of 1-, 2-, and 4-Day 1% LCA-Fed Mice

	Control (n = 6)	1-day LCA (n = 5)	2-day LCA (n = 5)	4-day LCA (n = 8)
ALT (U/L)	83 ± 42	102 ± 47	2398 ± 2278	4837 ± 1884*
AP (U/L)	220 ± 65	165 ± 58	536 ± 323	1334 ± 555*
Bili tot (mg/dl)	0.15 ± 0.05	0.32 ± 0.13	0.62 ± 0.33	2.33 ± 1.02*
SBA (μmol/L)	21 ± 25	16 ± 4	70 ± 67	280 ± 118*

*$P < 0.05$ compared with standard diet-fed controls (ANOVA with Bonferroni post testing).
Values are expressed as mean ± SD. ALT, alanine aminotransferase; Bili tot, total bilirubin; SBA, serum bile acids.

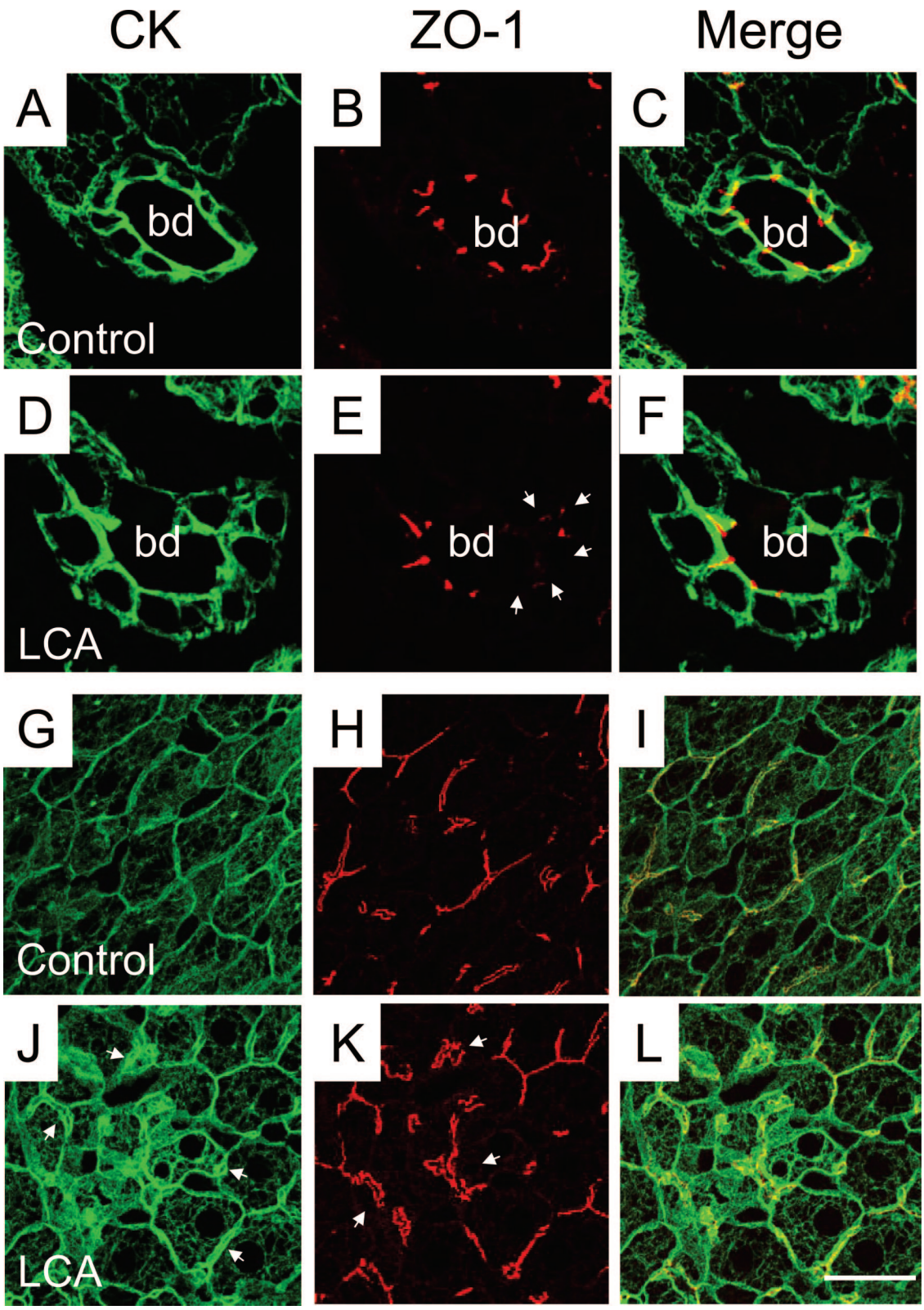

Figure 6. Tight junctions are altered in LCA-fed mouse liver. Double-immunofluorescence labeling for CK8/18 (in green) and the tight junction protein ZO-1 (in red) in control liver (**A–C** and **G–I**) and the liver from a 4-day LCA-fed mouse (**D–F** and **J–L**). **B** and **C:** ZO-1 staining of bile ducts in control diet-fed mice shows a distinct pattern outlining the cell contacts between BECs. **E** and **F:** In contrast, the liver of a 4-day LCA-fed mouse shows strikingly altered tight junctions morphologically characterized by partially disrupted and missing ZO-1 staining (**arrowheads**). Note also that BECs still form an intact epithelial monolayer (**D** and **F**), suggesting that the observed missing ZO-1 staining is not related to BEC necrosis. **G–I:** Staining of the intermediate filament network and tight junctions of hepatocytes in control diet-fed mice. **J:** The liver of a 4-day LCA-fed mouse shows a significantly increased density of the cytokeratin intermediate filament (CK-IF) network with a pronounced pericanalicular sheath (**arrowheads**). **K:** Strikingly altered tight junctions between hepatocytes in 4-day LCA-fed mouse liver morphologically characterized by elongation and distortions of the ZO-1 staining pattern (**arrowheads**). bd, bile duct. Bar = 10 μm.

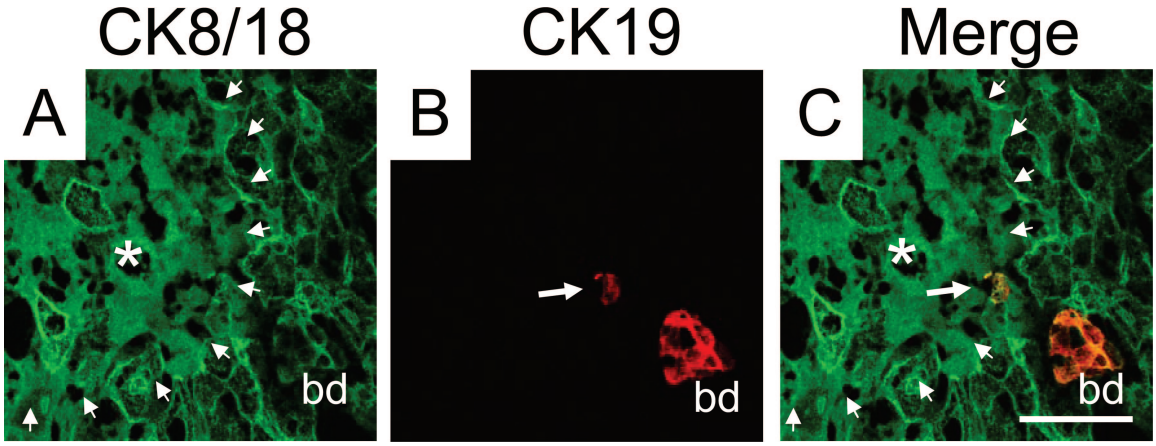

Figure 7. Rupture of the cholangioles (canals of Hering) and bile infarcts in LCA-fed mouse liver. **A–C:** Double-immunofluorescence labeling with CK8/18 (green) and CK19 (red) antibodies in the liver of a 2-day LCA-fed mouse. **A:** Degraded CK-IF network of hepatocytes in a bile infarct (marked with an **asterisk** and outlined by **arrowheads**) close to a portal tract with a bile duct (bd). **B:** CK19 antibody marks a bile duct (bd) and a canal of Hering (**arrow**) composed by two cholangiocytes. **C:** Note ruptured canal of Hering (**arrow**) on the margin of the bile infarct (marked with an **asterisk** and outlined by **arrowheads**). Bar = 50 μm.

Bacterial Counts of Liver and Spleen

To determine the possible role of bacterial translocation in the pathogenesis of LCA-induced liver injury in mice, bacterial counts of liver and spleen were performed as previously described.[19]

Measurement of Hepatic Hydroxyproline Content

To quantify liver fibrosis, hepatic hydroxyproline content was determined. The right liver lobe was homogenized in 6 N HCl (200 mg liver tissue/4 ml HCl) and hydrolyzed at 110°C for 16 hours. After filtration, 50 μl was added to 450 μl of 2.2% NaOH dissolved in citrate-acetate buffer (50 g of citric acid × H_2O, 12 ml of acetic acid, 120 g of sodium acetate × 3 H_2O, 34 g of NaOH, and 1 L of distilled water; pH 6.0). After neutralization, 250 μl of chloramin T solution was added and incubated for 20 minutes. After adding 250 μl of perchloric acid and 12 minutes of incubation at room temperature, 250 μl of *p*-dimethylaminobenzaldehyde solution was added and incubated at 60°C for 20 minutes. Hydroxyproline content was measured at 565 nm using a hydroxyproline standard curve.

Statistical Analysis

Data are reported as arithmetic means ± SD of five to eight animals in each group. Statistical analysis was performed using Student's *t*-test when appropriate or analysis of variance with Bonferroni post test when three or more groups were compared using the Sigmastat statistics program (Jandel Scientific, San Rafael, CA). A P value <0.05 was considered significant.

Results

LCA Feeding Leads to Bile Infarcts, Destructive Cholangitis, and Periductal Fibrosis

Beginning at day 2, livers of LCA-fed mice contained numerous bile infarcts (Figures 1 and 2A) that were morphologically indistinguishable from those seen in CBDL mice.[18,25] Small interlobular bile ducts were frequently obstructed with crystals, as revealed by electron microscopy (Figure 3, A and B). In addition, crystals penetrating into bile duct epithelial cells (BECs) were also observed (Figure 3C), suggesting that direct physicochemical LCA-induced injury of BECs may be important. The lobular lesions (ie, bile infarcts and single cell necroses) (Figure 2A) displayed light microscopic and ultrastructural characteristics of oncotic hepatocytes with hydropic swelling and disruption of cell and organelle membranes (not shown) as defined recently.[26] In addition, crystals were also deposited within bile infarcts (Figure 3D). These findings suggest that bile infarcts and bile ducts are faced with the highest LCA concentration within the liver. Around days 3 and 4, animals developed a dense neutrophilic-granulocytic infiltrate around small interlobular (Figure 2B) and larger bile ducts (Figure 2, C–F). This observation was further confirmed by the finding of numerous CD11b-positive periductal cells in LCA-fed mice as shown in Figure 4B. BECs were irregular with enlarged nuclei and focal pseudopapillary proliferations (Figure 2, C–E). In addition, subepithelial fluid accumulation lifting the epithelial cell layer (Figure 2, C and D) followed by ulceration of the bile duct epithelium (Figures 2, E and F, and 3, E and F) and pronounced periductal edema was frequently observed in larger ducts. There was no evidence for apoptosis of BECs because we found neither BECs with activated caspase-3 nor BECs with characteristic CK intermediate filament alterations typical for apoptotic cell death[18] (not shown), suggesting that necrosis may represent the primary mode of BEC death in our

model. These morphological findings were accompanied by a continuous increase in serum alanine aminotransferase levels followed by elevations of alkaline phosphatase and bilirubin (Table 1). Prolonged feeding of 1% LCA-supplemented diet beyond 7 days was associated with substantial mortality, indicating that continuous long-term treatment of this dose is not feasible (Figure 5). The acute cholangitis with neutrophils raised the possibility of a bacterial etiology related to increased bacterial translocation from the gut into the liver and spleen. However, we found no differences in bacterial counts in livers and spleens between LCA-fed mice and controls (data not shown). The development of pericholangitis in LCA-fed mice led to the hypothesis that this could be due to leakage of the tight junctions of BECs. As determined by immunofluorescence microscopy with staining for tight junction protein ZO-1 (Figure 6, E and F) and by electron microscopy (Figure 3, E and F), tight junctions were irregular and focally disrupted, suggesting that bile ducts were leaky under these experimental conditions. Time course studies revealed that tight junction alterations preceded lifting and ulceration of the epithelial cell layer, suggesting that tight junction alterations may be of primary importance in LCA-induced cholangiopathy. Tight junctions between hepatocytes also showed alterations of the ZO-1 pattern with distortion and widening indicative of dilated canaliculi (Figure 6, K and L).

Moreover, we frequently observed ruptured canals of Hering in the proximity to bile infarcts (Figure 7), parallel to previous observations in CBDL mice.[18] The evolving cholangitis in LCA-fed mouse liver was accompanied by a significantly increased number of α-SMA-positive periductal myofibroblasts (Figure 8C) responsible for an astonishingly rapidly evolution and pronounced periductal fibrosis (Figure 8D) comparable with previous observations in *Mdr2* knockout mice.[19] In addition, α-SMA protein levels were significantly increased in LCA-fed mice compared with controls (Figure 8E). Increased proliferation of periductal myofibroblasts was also demonstrated by a significantly increased number of Ki-67-positive (CK19-negative) periductal myofibroblasts (Figure 9). Liver fibrosis was confirmed biochemically by significantly higher hepatic hydroxyproline content in LCA-fed mice after 4 days (ie, 194 $\pm$ 24 vs. 104 $\pm$ 4 mg/g liver in controls; $P > 0.05$). This was accompanied by a significantly enhanced expression of collagen 1a1 mRNA (52-fold) compared with controls (Table 2). Of interest, the absolute increase of TIMP-1 mRNA expression (424-fold) was greater than for MMP-2 mRNA (10-fold), suggesting that liver fibrosis in LCA-fed mice may, at least in part, result from increased matrix production in the presence of decreased matrix degradation (Table 2). Taken together these findings support the concept that LCA feeding in mice results in partial biliary obstruction and subsequently bile infarcts. In addition, these findings suggest that LCA-induced alterations of tight junctions caused destructive cholangitis and activation of BECs, initiating proliferation and activation of periductal myofibroblasts and leading to periductal fibrosis.

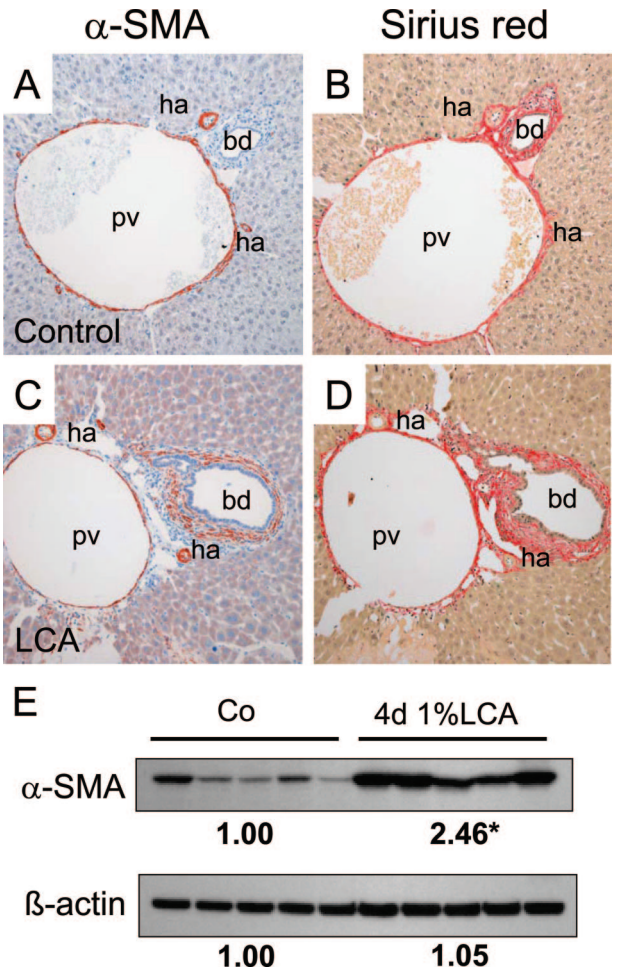

Figure 8. Periductal fibrosis in LCA-fed mouse liver. Immunohistochemistry (**A** and **C**) for α-SMA-positive cells and Sirius red staining (**B** and **D**) for collagen in control liver (**A** and **B**) and in the liver from a 4-day LCA-fed mouse (**C** and **D**). **A:** In the control liver, only smooth muscle cells of the hepatic artery branches (ha) and the portal vein (pv) are α-SMA positive. **C:** In contrast, there are numerous α-SMA-positive myofibroblasts surrounding the bile duct (bd) of a 4-day LCA-fed mouse. Note that hepatic arteries and portal veins of the control liver and 4-day LCA-fed mice are of the same size, indicating that both situations are cut at the same level of the biliary tree. **B** and **D:** Sirius red staining outlines the pronounced periductal fibrosis in the LCA-fed mouse liver. Original magnification, $\times$20. **E:** Protein quantification for α-SMA and β-actin by Western blotting in control livers (CO) and livers from 4-day LCA-fed mice (4-day 1% LCA). Note the significant increased α-SMA and unchanged β-actin expression in LCA-fed mouse liver. Densitometry data are expressed as the fold change relative to control diet-fed animals. Values are the means from five animals in each group. $^*P < 0.05$ compared with standard diet-fed controls (Student's *t*-test).

Comparison of the Lobular Distribution of Fluorescent UDCA and India Ink in LCA-Fed Mice and CBDL Mice: Clues to the Pathogenesis of the Cholestatic Phenotype

Because bile infarcts were frequently observed in proximity to disrupted canals of Hering (Figure 7), we searched for communications between the bile duct system and bile infarcts as previously seen in CBDL mice.[18] Fluorescent UDCA injected into the inferior vena cava was rapidly secreted into canaliculi and bile ducts in CBDL and LCA-fed mice (Figure 10, A and C) After retrograde injection into the common bile duct, India ink

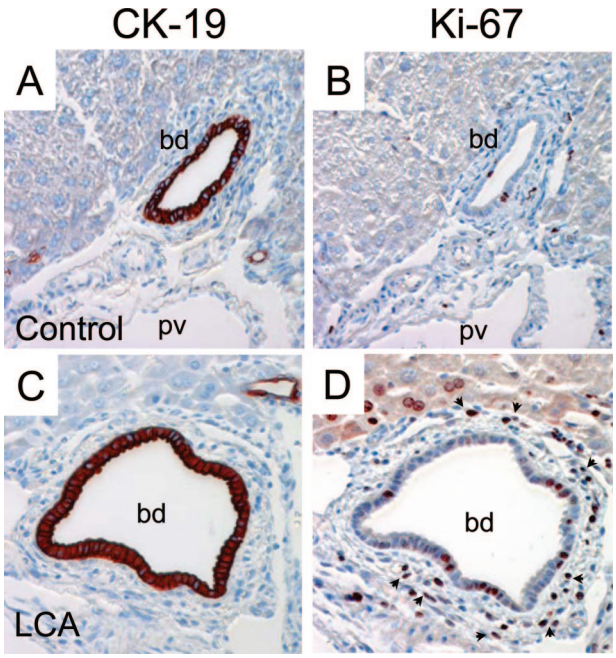

Figure 9. Proliferation of periductal myofibroblasts and bile duct epithelial cells in LCA-fed mouse liver. Immunohistochemistry for (**A** and **C**) CK19-positive cholangiocytes and proliferation marker Ki-67 (**B** and **D**). **B:** In the control liver, only some positive nuclei are seen in the portal field. **D:** In contrast, there are numerous Ki-67-positive (CK19-negative) periductal myofibroblasts surrounding the bile duct and also few proliferating Ki-67-positive BECs in LCA-fed mouse liver. bd, bile duct. Original magnification, ×40.

filled bile ducts and bile canaliculi and accumulated in bile infarcts (Figure 10B). On the other hand, in LCA-fed mice, India ink filled bile ducts but accumulated in only few bile infarcts (Figure 10D). Taken together, these findings support our concept 1) that bile infarcts have connection to the bile duct system, 2) that bile infarcts contain high concentrations of bile acids, and 3) most importantly, that these experiments are consistent with partial biliary obstruction in LCA-fed mice.

LCA Feeding Leads to Adaptive Hepatocellular Transporter and Metabolic Enzyme Expression in Mice

To study the functional importance of the described partial biliary obstruction, we determined bile flow in LCA-fed mice on days 1 and 4 (Table 3). Bile flow tended to increase on day 1 and was significantly decreased on day 4. After an initial increase on day 1, biliary secretion of cholesterol, phospholipids, glutathione, and bile acids was significantly reduced in LCA-fed mice. The predominating bile acids in bile were LCA and chenodeoxycholic acid (Table 4).

Because previous studies in isolated-perfused rat liver[27,28] have indicated significant alterations in expression and localization of ABC transporter proteins, which may, at least in part, explain cholestasis in LCA-treated rodents, we studied hepatobiliary transport proteins in our model. LCA feeding led to a significant reduction in the expression of the main basolateral bile acid uptake systems Ntcp and Oatp1 (Figures 11 and 12B). Canalicular

Table 2. Hepatic mRNA Expression of Several Genes in 4-Day 1% LCA-Fed Mice

	Control (n = 5)	4-day 1% LCA (n = 5)
Collagen 1a1	1.00 ± 0.62	51.7 ± 43.6*
TIMP-1	1.00 ± 0.41	424 ± 233*
MMP-2	1.00 ± 0.23	9.5 ± 6.3*
Ntcp	1.00 ± 0.28	0.26 ± 0.10*
Bsep	1.00 ± 0.56	1.19 ± 0.47
Mrp2	1.00 ± 0.61	0.83 ± 0.23
Mrp3	1.00 ± 0.94	3.10 ± 1.03
Cyp3a11	1.00 ± 0.89	3.33 ± 2.18
Cyp7a1	1.00 ± 0.84	0.07 ± 0.04*
Cyp8b1	1.00 ± 0.33	0.03 ± 0.01*
Sult2a1	1.00 ± 0.96	7.11 ± 2.69*

*$P < 0.05$ compared with standard diet-fed controls (Student's t-test).

Values are normalized to controls as 1.00 and 28S rRNA expression and are expressed as mean ± SD.

Bsep protein levels and localization were not altered in LCA-fed mice compared with controls (Figures 11 and 13 B), and there was no evidence of canalicular mistargeting or retrieval of Bsep (Figure 13, E and F). Total Mrp2 protein levels were also unchanged in LCA-fed mice (Figure 11), but the expression of Mrp2 protein was limited to acinar zone 3 (Figure 13, H and I), where it remained localized to the canalicular membrane (Figure

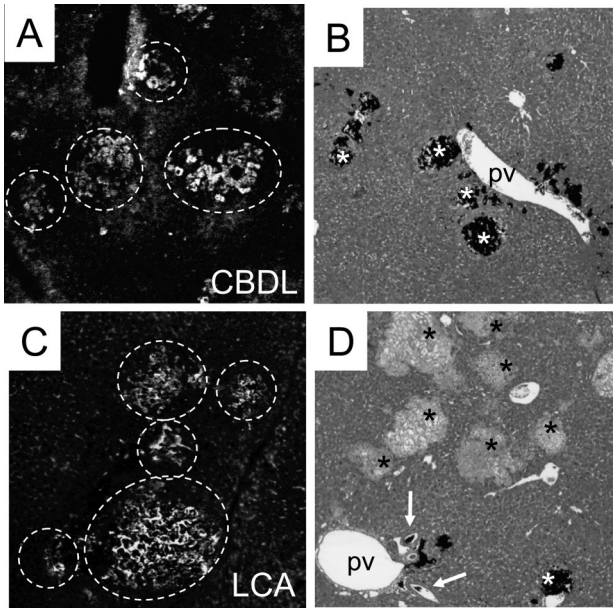

Figure 10. Bile infarcts in LCA-fed mouse liver fill-up with fluorescent UDCA injected into the inferior vena cava, but partial obstruction of the biliary tree prevents retrograde filling of bile infarcts with India ink. Fluorescent UDCA injected into the inferior vena cava (**A** and **C**) and India ink injected into the common bile duct (**B** and **D**) in livers from CBDL mice (**A** and **B**) and 4-day LCA-fed mice (**C** and **D**). **A** and **C:** Bile infarcts in CBDL and LCA-fed mouse livers are impregnated by fluorescent UDCA, suggesting that fluorescent UDCA is secreted into bile canaliculi and regurgitates into bile infarcts (surrounded by the white circles) due to outflow obstruction in both models. **B:** India ink injected into the common bile duct after CBDL fills most bile infarcts (**white asterisks**). **D:** India ink injected into the common bile duct enters interlobular bile ducts (**arrows**) in LCA-fed mouse. India ink stains only the minority of bile infarcts (**white asterisk**), whereas most remain negative for India ink (**black asterisks**), suggesting that partially biliary obstruction prevents complete retrograde filling of bile infarcts with India ink in LCA-fed mice. Original magnification, ×10.

Table 3. Bile Flow and Biliary Output Rates in 1- and 4-Day 1% LCA-Fed Mice

	Bile flow (μL g^{-1} LW min^{-1})	Cholesterol (mmol g^{-1} LW min^{-1})	Phospholipids (mmol g^{-1} LW min^{-1})	Glutathione (nmol g^{-1} LW min^{-1})	Bile acids (mmol g^{-1} LW min^{-1})
Control (n = 6)	1.6 ± 0.4	0.4 ± 0.1	4.1 ± 0.9	6.0 ± 2.0	30.6 ± 7.7
1-day LCA (n = 6)	1.7 ± 0.5	0.9 ± 0.3	7.7 ± 1.5*	7.2 ± 1.8	72.2 ± 10.9*
4-day LCA (n = 6)	0.6 ± 0.4*†	0.3 ± 0.2†	2.4 ± 1.9†	2.7 ± 2.2†	19.1 ± 15.2†

*$P < 0.05$ compared with standard diet-fed controls; †$P < 0.05$ 1- versus 4-day LCA (ANOVA with Bonferroni post test).
Values are expressed as mean ± SD. LW, liver weight.

13, K and L). These data suggest that the observed reduction in biliary glutathione secretion in LCA-fed mice (Table 3) was related to impaired Mrp2 expression in acinar zone 1 and 2. Basolateral Mrp3 expression was significantly induced by LCA feeding (Figures 11 and 12D). Interestingly, reduced Ntcp staining was reciprocally accompanied by enhanced Mrp3 staining in LCA-fed mouse liver (Figure 12). The changes in transporter protein levels were accompanied by respective changes in mRNA expression (Table 3), indicating that these changes may be mediated largely at a transcriptional level. However, these findings do not exclude additional posttranscriptional effects of LCA. Expression of Sult2a1 was also induced in LCA-fed mice (Table 2), indicating that LCA-fed mice may, at least in part, metabolize LCA by sulfation.

Discussion

The emerging interest in the molecular mechanisms of bile acid transport and detoxification has resulted in several studies on LCA-induced liver injury in knockout mice for nuclear receptors and their respective target genes.[10–15] These studies have mainly focused on specific molecular aspects of LCA detoxification, whereas the cholestatic phenotype induced by LCA remains functionally and morphologically poorly understood.[29,30] Moreover, the critical question arises of whether feeding

Table 4. Biliary Bile Acid Composition in Control and LCA-Fed Mice

Bile acid	Control (n = 3) (%)	4-day 1% LCA (n = 5) (%)
LCA	Not detectable	13.1 ± 3.0*
DCA	2.7 ± 2.0	2.1 ± 1.5
allo-CA	4.2 ± 1.0	1.8 ± 0.3*
CDCA	1.2 ± 0.2	35.7 ± 7.2*
α-MCA	2.4 ± 0.4	18.2 ± 3.4*
HDCA	Not detectable	9.9 ± 1.8*
CA	53.2 ± 5.8	7.6 ± 5.3*
UDCA	0.7 ± 0.2	3.2 ± 2.1
12α-OI, 3-one	9.0 ± 1.7	2.3 ± 0.7*
β-MCA	7.9 ± 1.4	2.5 ± 1.3*
7α-OI, 3-one	2.1 ± 0.9	0.7 ± 0.8
ω-MCA	10.7 ± 1.9	1.8 ± 0.9*
Other	6.0 ± 2.6	1.1 ± 1.7

*$P < 0.05$ LCA-fed mice compared with standard diet-fed controls (Student's t-test).

1% LCA was fed for 4 days. Controls received a standard chow. Values are percentages (expressed as mean ± SD). CA, cholic acid; CDCA, chenodeoxycholic acid; DCA, deoxycholic acid; HDCA, hyodeoxycholic acid; LCA, lithocholic acid; MCA, muricholic acid.

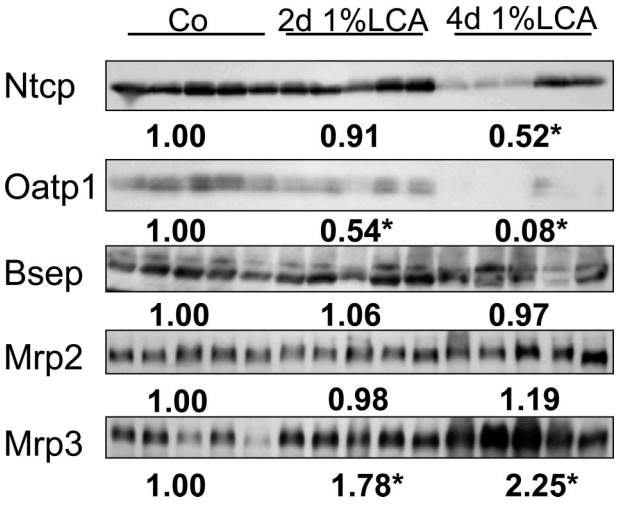

Figure 11. Effects of LCA feeding on hepatic Ntcp, Oatp1, Bsep, Mrp2, and Mrp3 protein levels. Liver membranes were isolated from control diet-fed (Co) and 1% (w/w) LCA (for 2 and 4 days)-fed mice and analyzed by Western blotting. Densitometry data are expressed as the fold change relative to control diet-fed animals. Values are the means from five animals in each group. There is a significant decrease in Ntcp and Oatp1 concomitant with a significant increase in Mrp3 protein levels in LCA-fed mice, whereas no significant differences in Bsep and Mrp2 protein levels were observed.

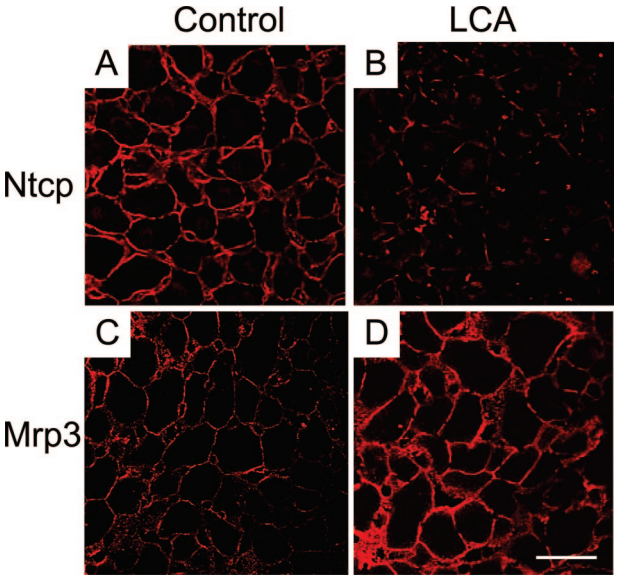

Figure 12. Reciprocal Ntcp and Mrp3 tissue localization in LCA-fed mouse liver. Ntcp (**A** and **B**) and Mrp3 (**C** and **D**) tissue localization was compared between control (**A** and **C**) and 1% (w/w) LCA-fed (for 4 days) (**B** and **D**) mouse livers (both red). Significantly reduced Ntcp staining (**C**) and enhanced Mrp3 staining (**D**) are seen in LCA-fed mouse liver. Bar = 20 μm.

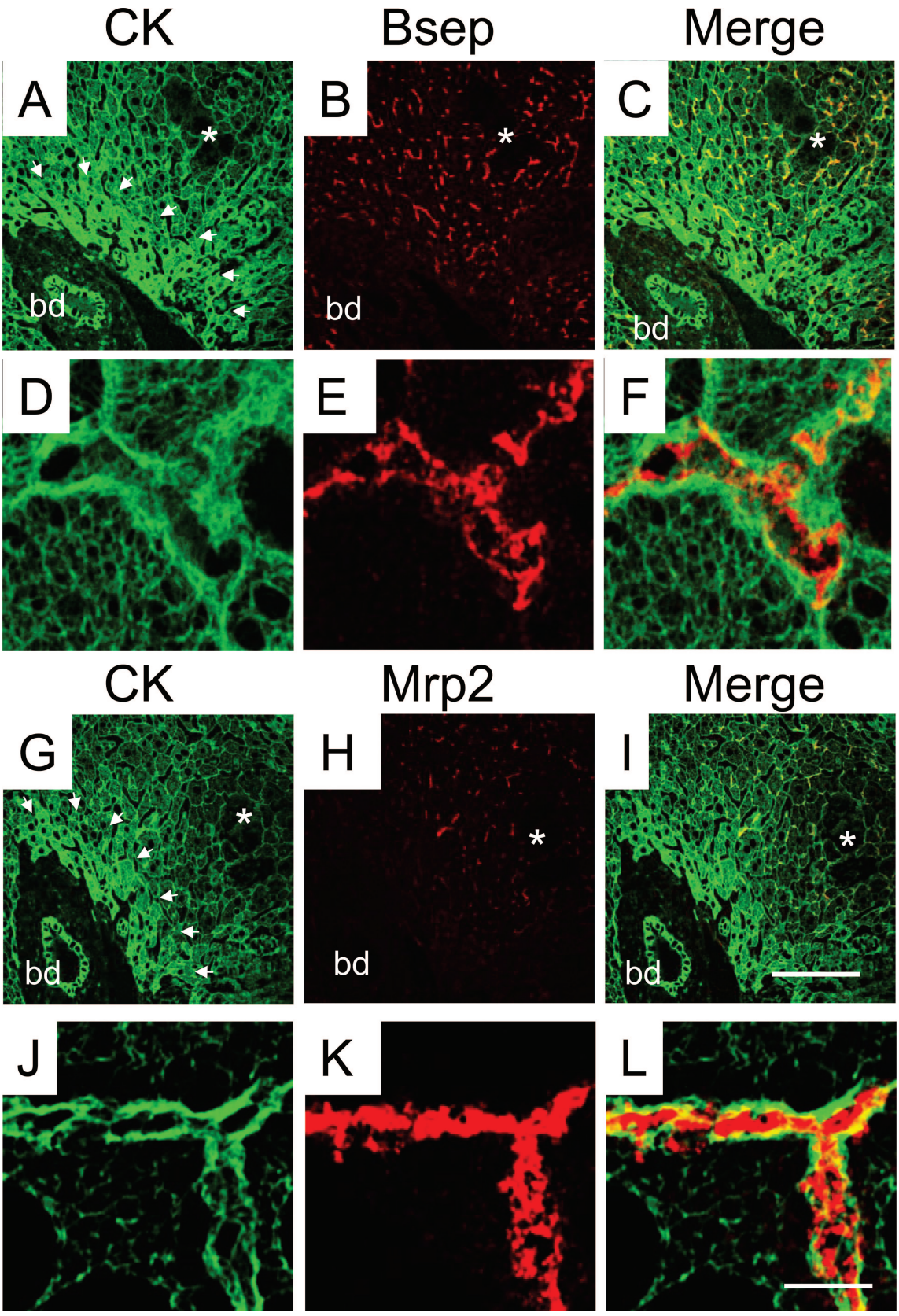

Figure 13. Bsep expression is preserved throughout the liver lobule, whereas Mrp2 expression is restricted to acinar zone 3 in LCA-fed mouse liver. Double-immunofluorescence labeling of CKs (green; **A, C, D, F, G, J, I,** and **L**) and Bsep (**B, C, E,** and **F**) or Mrp2 (**H, I, K,** and **L**) (red) in 1% (w/w) LCA-fed (for 4 days) mouse liver. **B** and **C:** Bsep expression is preserved throughout the liver lobule in LCA-fed mouse liver. **H** and **I:** In contrast, Mrp2 expression is reduced to hepatic acinar zone 3. **A** and **G:** Note also the increased density of the CK-IF network in acinar zone 1 (indicated by the **arrowheads**). **E, F, K,** and **L:** Note that there is no evidence for canalicular retrieval or targeting defect for Bsep and Mrp2 in LCA-fed mouse liver. bd, bile duct. Bar for **A–C** and **G–I** = 100 μm. Bar for **D–F** and **J–L** = 5 μm.

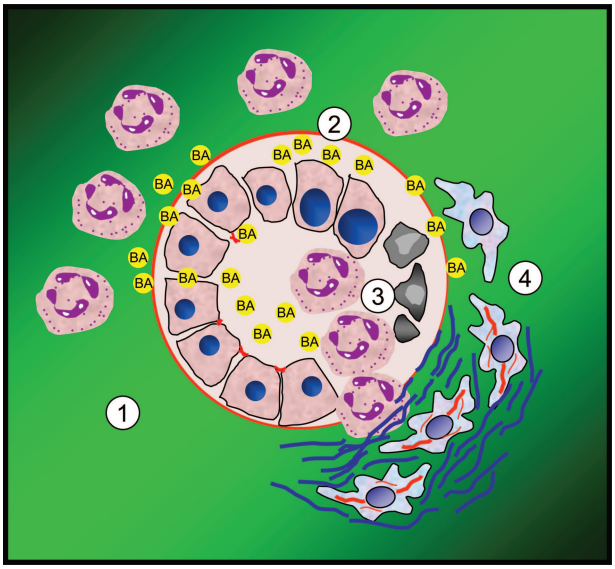

Figure 14. Suggested sequence of events of cholangiopathy in LCA-fed mice—further evidence for the toxic bile concept. 1) LCA feeding leads to alterations of tight junctions of BECs, resulting in leaky bile ducts and chemotaxis of neutrophil granulocytes. 2) Inflammation and extravasation of toxic bile lead to subepithelial fluid accumulation and concomitant detachment of the biliary epithelium resulting in lifting of the epithelial cell layer. 3) Neutrophil granulocytes invade the bile duct lumina via transmigration and ulcerations of the epithelial cell layer. 4) Ongoing efflux of toxic bile into the portal field together with activation of BECs leads to proliferation and activation of periductal myofibroblasts resulting in rapidly evolving periductal fibrosis.

of a toxic bile acid is capable of inducing bile duct injury as the primary mechanism of hepatotoxicity. We herein show that feeding hydrophobic LCA to mice induces partial bile duct obstruction, bile infarcts, destructive cholangitis, and periductal fibrosis within days (Figure 14).

What Is the Pathogenesis of Cholestasis in LCA-Fed Mice?

In the past, many pathogenetic mechanisms of cholestasis in LCA-treated rodents (ie, mainly rats) have been proposed,[3,5–9] and most of these studies have concluded that LCA-induced cholestasis is canalicular in origin. We herein demonstrate that cholestasis in LCA-fed mouse liver results from partial obstruction of bile ducts by crystals (presumably LCA precipitates). This novel conclusion is also supported by the described differential distribution pattern of biliary-secreted fluorescent UDCA and India ink, injected into the common bile duct, in LCA-fed and CBDL mice. In addition, we found that Bsep expression was preserved and there was no evidence for canalicular retrieval of this transporter. Mrp2 tissue protein levels were unchanged, but its localization was limited to acinar zone 3, which could explain reduced biliary glutathione excretion in our model. Moreover, expression of Ntcp and Oatp1 was significantly reduced whereas Mrp3 (accompanied by Sult2a1 overexpression) was induced in response to LCA feeding, suggesting that these findings reflect an adaptive response protecting hepatocytes from ongoing hepatocellular accumulation of bile acids as previously observed in CBDL mice.[22] Although it cannot be entirely excluded that these transporter alterations may be directly caused by LCA, the findings of the current study are consistent with the alterations of hepatic transport systems observed previously in mice and rats with obstructive cholestasis due to common bile duct ligation.[22,31–33] Thus, it is unlikely that the transporter alterations observed in the current study are the primary cause for cholestasis in LCA-fed mice but rather may represent a secondary adaptive response to the cholestatic phenotype.

Why Do LCA-Fed Mice Develop Bile Infarcts?

Bile infarcts defined as confluent periportal liver cell necrosis with retained pigment material are a characteristic type of liver cell damage in response to obstructive cholestasis in humans and related animal models (eg, CBDL in rodents).[25] We have previously shown that maintained bile secretion and increased biliary pressure are critical determinants for the development of bile infarcts in CBDL mice and that these lesions result from rupture of the canals of Hering[18,22] with exposure of hepatocytes to bile acid concentrations in the millimolar range derived from bile leaking into the liver parenchyma.[34] The development of bile infarcts in LCA-fed mice (recently also described in intraperitoneally treated mice[10,11]) resulting from leaky, disrupted cholangioles (canals of Herring) may have previously been misinterpreted as "hemorrhagic cysts resembling peliosis hepatis" by Bagheri et al[29] in LCA-treated rats. Our concept is confirmed by the finding of LCA crystals within bile infarcts. This hypothesis is further supported by the fact that most bile infarcts in LCA-treated mice remained unstained by India ink injected retrogradely into the common bile duct (which contrasts the findings in CBDL mice). On the other hand, biliary (orthogradely) excreted fluorescent UDCA accumulated in bile infarcts as observed in LCA-fed animals. Both observations may primarily be related to proximal bile duct obstruction in LCA-fed mice. In addition, previous studies by Benedetti et al[35] also suggested an obstructive component of LCA-induced cholestasis, at least in the isolated perfused rat liver.

Why Do LCA-Fed Mice Develop Destructive Cholangitis?

Because bile infarcts and destructive cholangitis are the morphological hallmarks of the cholestatic phenotype in LCA-fed mouse liver, it is most likely that the bile ducts represent an important Achilles' heel in regard to the hepatoxic potential of bile acids in mice analogous to our previous findings in *Mdr2*$^{-/-}$ mice.[18,19] LCA appears to provoke cholangitis through its physicochemical properties, ie, high hydrophobicity and lithogenicity. The perception that bile duct obstruction in LCA-fed mice may be caused by LCA precipitates is also supported by the fact that bile duct stones previously observed in chronically LCA-fed rats primarily consist of LCA.[2] Because we observed intraductal LCA crystals damaging BECs and

finally resulting in ulcerations, it is reasonable to assume that cholangitis is directly related to the local toxic effects of LCA in mouse liver.[2,36] However, it cannot be excluded from the presented data that an LCA-induced inflammatory response of BECs could additionally perpetuate cholangitis and proliferation of periductal myofibroblasts resulting in periductal fibrosis (eg, via inducing cytokine/chemokine production in BECs).[16] In addition, based on the recent observation of toxic bile acid-induced hepatic stellate cell proliferation by Svegliati-Baroni et al,[37] it is attractive to speculate that the observed proliferation of periductal myofibroblasts in LCA-fed mice could also be directly related to bile acids. The demonstrated induction of collagen 1a1, together with the greater induction of TIMP-1 in relation to MMP-2, suggests that liver fibrosis in LCA-fed mice could result, at least in part, from increased matrix production in the presence of decreased matrix degradation. Because the prolonged feeding of 1% LCA-supplemented diet resulted in a detrimental outcome, future studies will have to determine whether alternative feeding protocols (eg, alternating periods of LCA and standard-diet feeding) are also able of producing parenchymal liver fibrosis and ultimately cirrhosis.

Do These Experimental Findings Have Potential Implications for Human Liver Disease?

The novel finding that LCA feeding in mice induces destructive cholangitis supports the concept that "toxic" bile is able to induce cholangitis and consequently periductal fibrosis.[19] Despite the fact that there is no proof for a causative role of LCA in human cholestatic liver diseases, LCA has been used since the early 1960s in experimental models to study cholestasis. However, because we observed crystals in cholangioles, bile ducts, and bile infarcts detected by electron microscopy, such crystals may have been missed in previous studies in fixed liver samples (ie, solubilization of LCA crystals during formalin fixation). Therefore, it may also be worthwhile to perform ultrastructural studies of bile ducts and their contents in human liver samples (eg, liver explants).

In summary, we provide evidence that the cholestatic phenotype in LCA-fed mouse liver is the result of LCA-induced obstruction of bile ducts and suppurative cholangitis leading to periductal fibrosis (Figure 14). This is accompanied by an adaptive transporter and enzyme response. This information should be valuable for understanding LCA-treated mice as a model system for cholestatic liver diseases.

Acknowledgments

The rat anti Troma-III antibody developed by Rolf Kemler (Max Planck Institute, Freiburg, Germany) was obtained from the Developmental Studies Hybridoma Bank developed under the auspices of the National Institute of Child Health and Human Development and maintained by the University of Iowa (Iowa City, IA). Antibodies against Mrp2 and Ntcp were kindly provided by Dr. Bruno Stieger (Zurich, Switzerland), against Bsep by Dr. Renxue Wang (Vancouver, Canada), and against Mrp3 by Dr. Dietrich Keppler (Heidelberg, Germany). We gratefully acknowledge Dr. W. Erwa (Graz) and colleagues for performing biochemical analysis of serum liver tests. The excellent technical assistance of Judith Gumhold and Dagmar Silbert (Graz) is also gratefully acknowledged. We thank Dr. Alan Hofmann (San Diego, CA) for fruitful discussions and helpful suggestions.

References

1. Hofmann AF: Detoxification of lithocholic acid, a toxic bile acid: relevance to drug hepatotoxicity. Drug Metab Rev 2004, 36:703–722
2. Palmer RH, Ruban Z: Production of bile duct hyperplasia and gallstones by lithocholic acid. J Clin Invest 1966, 45:1255–1267
3. Miyai K, Richardson AL, Mayr W, Javitt NB: Subcellular pathology of rat liver in cholestasis and choleresis induced by bile salts: 1. Effects of lithocholic, 3beta-hydroxy-5-cholenoic, cholic, and dehydrocholic acids. Lab Invest 1977, 36:249–258
4. Hofmann AF: The continuing importance of bile acids in liver and intestinal disease. Arch Intern Med 1999, 159:2647–2658
5. Kakis G, Yousef IM: Pathogenesis of lithocholate- and taurolithocholate-induced intrahepatic cholestasis in rats. Gastroenterology 1978, 75:595–607
6. Kakis G, Phillips MJ, Yousef IM: The respective roles of membrane cholesterol and of sodium potassium adenosine triphosphatase in the pathogenesis of lithocholate-induced cholestasis. Lab Invest 1980, 43:73–81
7. Bonvicini F, Gautier A, Gardiol D, Borel GA: Cholesterol in acute cholestasis induced by taurolithocholic acid: a cytochemical study in transmission and scanning electron microscopy. Lab Invest 1978, 38:487–495
8. Kubitz R, Sutfels G, Kuhlkamp T, Kolling R, Haussinger D: Trafficking of the bile salt export pump from the Golgi to the canalicular membrane is regulated by the p38 MAP kinase. Gastroenterology 2004, 126:541–553
9. Beuers U, Denk GU, Soroka CJ, Wimmer R, Rust C, Paumgartner G, Boyer JL: Taurolithocholic acid exerts cholestatic effects via phosphatidylinositol 3-kinase-dependent mechanisms in perfused rat livers and rat hepatocyte couplets. J Biol Chem 2003, 278:17810–17818
10. Staudinger JL, Goodwin B, Jones SA, Hawkins-Brown D, MacKenzie KI, LaTour A, Liu Y, Klaasen CD, Brown KK, Reinhard J, Willson TM, Koller BH, Kliewer SA: The nuclear receptor PXR is a lithocholic acid sensor that protects against liver toxicity. Proc Natl Acad Sci USA 2001, 98:3369–3374
11. Xie W, Radominska-Pandya A, Shi Y, Simon CM, Nelson MC, Ong ES, Waxmann DJ, Evans RM: An essential role for nuclear receptors SXR/PXR in detoxification of cholestatic bile acids. Proc Natl Acad Sci USA 2001, 98:3375–3380
12. Sinal CJ, Tohkin M, Miyata M, Ward JM, Lambert G, Gonzalez FJ: Targeted disruption of the nuclear receptor FXR/BAR impairs bile acid and lipid homeostasis. Cell 2000, 102:731–744
13. Kitada H, Miyata M, Nakamura T, Tozawa A, Honma W, Shimada M, Nagata, Sinal CJ, Guo GL, Gonzalez FJ, Yamazoe Y: Protective role of hydroxysteroid sulfotransferase in lithocholic acid-induced liver toxicity. J Biol Chem 2003, 278:17838–17844
14. Schuetz EG, Strom S, Yasuda K, Lecureur V, Assem M, Brimer C, Lamba J, Kim RB, Ramachandran V, Komoroski BJ, Venkataramanan R, Cai H, Sinal CJ, Gonzalez FJ, Schuetz JD: Disrupted bile acid homeostasis reveals an unexpected interaction among nuclear hormone receptors, transporters, and cytochrome P450. J Biol Chem 2001, 276:39411–39418
15. Saini SP, Sonoda J, Xu L, Toma D, Uppal H, Mu Y, Ren S, Moore DD, Evans RM, Xie W: A novel constitutive androstane receptor-mediated and CYP3A-independent pathway of bile acid detoxification. Mol Pharmacol 2004, 65:292–300
16. Lazaridis KN, Strazzabosco M, LaRusso NF: The cholangiopathies: disorders of biliary epithelia. Gastroenterology 2004, 127:1565–1577

17. Trauner M, Boyer JL: Bile salt transporters: molecular characterization, function, and regulation. Physiol Rev 2003, 83:633–671
18. Fickert P, Zollner G, Fuchsbichler A, Stumptner C, Weiglein AH, Lammert F, Marshall HU, Tsybrovskyy O, Zatloukal K, Denk H, Trauner M: Ursodeoxycholic acid aggravates bile infarcts in bile duct-ligated and Mdr2 knockout mice via disruption of cholangioles. Gastroenterology 2002, 123:1238–1251
19. Fickert P, Fuchsbichler A, Wagner M, Zollner G, Kaser A, Tilg H, Krause R, Lammert F, Langner C, Zatloukal K, Marschall HU, Denk H, Trauner M: Regurgitation of bile acids from leaky bile ducts causes sclerosing cholangitis in Mdr2 (Abcb4) knockout mice. Gastroenterology 2004, 127:261–274
20. Lammert F, Wang DQ, Hillebrandt S, Geier A, Fickert P, Trauner M, Matern S, Paigen B, Carey MC: Spontaneous cholecysto- and hepatolithiasis in Mdr2−/− mice: a model for low phospholipids-associated cholelithiasis. Hepatology 2004, 39:117–128
21. Fickert P, Zollner G, Fuchsbichler A, Stumptner C, Pojer C, Zenz R, Lammert F, Stieger B, Meier PJ, Zatloukal K, Denk H, Trauner M: Effects of ursodeoxycholic and cholic acid feeding on hepatocellular transporter expression in mouse liver. Gastroenterology 2001, 121:170–183
22. Wagner M, Fickert P, Zollner G, Fuchsbichler A, Silbert D, Tsybrovskyy O, Zatloukal K, Guo GL, Schuetz JD, Gonzalez FJ, Marschall HU, Denk H, Trauner M: Role of farnesoid X receptor in determining hepatic ABC transporter expression and liver injury in bile duct-ligated mice. Gastroenterology 2003, 125:825–838
23. Bohan A, Chen WS, Denson LA, Held MA, Boyer JL: Tumor necrosis factor alpha-dependent up-regulation of Lrh-1 and Mrp3 (Abcc3) reduces liver injury in obstructive cholestasis. J Biol Chem 2003, 278:36688–36698
24. Zollner G, Fickert P, Fuchsbichler A, Silbert D, Wagner M, Arbeiter S, Gonzalez FJ, Marschall HU, Zatloukal K, Denk H, Trauner M: Role of nuclear bile acid receptor FXR, in adaptive ABC transporter regulation by cholic and ursodeoxycholic acid in mouse liver, kidney and intestine. J Hepatol 2003, 39:480–488
25. Fickert P, Trauner M, Fuchsbichler A, Stumptner C, Zatloukal K, Denk H: Cytokeratins as targets for bile acid-induced toxicity. Am J Pathol 2002, 160:491–499
26. Jaeschke H, Lemasters JJ: Apoptosis versus oncotic necrosis in hepatic ischemia/reperfusion injury. Gastroenterology 2003, 125:1246–1257
27. Crocenzi FA, Mottino AD, Sanchez Pozzi EJ, Pellegrino JM, Rodriguez Garay EA, Milkiewicz P, Vore M, Coleman R, Roma MG: Impaired localization and transport function of canalicular Bsep in taurolithocholate induced cholesteasis in the rat. Gut 2003, 52:1170–1177
28. Beuers U, Bilzer M, Chittattu A, Kullak-Ublick GA, Keppler D, Paumgartner G, Dombrowski F: Tauroursodeoxycholic acid inserts the apical conjugate export pump, Mrp2, into canalicular membranes and stimulates organic anion secretion by protein kinase C-dependent mechanisms in cholestatic rat liver. Hepatology 2001, 33:1206–1216
29. Bagheri SA, Bolt MG, Boyer JL, Palmer RH: Stimulation of thymidine incorporation in mouse liver and biliary tract epithelium by lithocholate and deoxycholate. Gastroenterology 1978, 74:188–192
30. Layden TJ, Schwarz, Boyer JL: Scanning electron microscopy of the rat liver: studies of the effect of taurolithocholate and other models of cholestasis. Gastroenterology 1975, 69:724–738
31. Lee J, Azzaroli F, Wang L, Soroka CJ, Gigliozzi A, Setchell KD, Kramer W, Boyer JL: Adaptive regulation of bile salt transporters in kidney and liver in obstructive cholestasis in the rat. Gastroenterology 2001, 121:1473–1484
32. Lee JM, Trauner M, Soroka CJ, Stieger B, Meier PJ, Boyer JL: Expression of the bile salt export pump is maintained after chronic cholestasis in the rat. Gastroenterology 2000, 118:163–172
33. Trauner M, Arrese M, Soroka CJ, Ananthanarayanan M, Koeppel TA, Schlosser SF, Suchy FJ, Keppler D, Boyer JL: The rat canalicular conjugate export pump (Mrp2) is down-regulated in intrahepatic and obstructive cholestasis. Gastroenterology 1997, 113:255–264
34. Fickert P, Trauner M, Fuchsbichler A, Zollner G, Wagner M, Marschall HU, Zatloukal K, Denk H: Oncosis represents the main type of cell death in mouse models of cholestasis. J Hepatol 2005, 42:378–385
35. Benedetti A, Alvaro D, Bassotti C, Gigliozzi A, Ferretti G, La Rosa T, Jezequel AM, Capocaccia L: Cytotoxicity of bile salts against biliary epithelium: a study in isolated bile ductule fragments and isolated perfused rat liver. Hepatology 1997, 26:9–21
36. Palmer RH: Bile acid sulfates: II. Formation, metabolism, and excretion of lithocholic acid sulfates in the rat. J Lipid Res 1971, 12:680–687
37. Svegliati-Baroni G, Ridolfi F, Hannivoort R, Saccomanno S, Homan M, De Minicis S, Jansen PL, Candelaresi C, Benedetti A, Moshage H: Bile acids induce hepatis stellate cell proliferation via activation of the epidermal growth factor receptor. Gastroenterology 2005, 128:1042–1055